AIAA JOURNAL
Vol. 45, No. 1, January 2007

Competing Broadband Noise Mechanisms in Low-Speed Axial Fans

Stéphane Moreau*
Valeo Motors and Actuators, 78321 La Verrière, France
and
Michel Roger†
Ecole Centrale de Lyon, 69134 Ecully, France

DOI: 10.2514/1.14583

This paper compares two broadband noise mechanisms, the trailing-edge noise or self-noise, and the leading-edge noise or turbulence-ingestion noise, in several blade technologies. Two previously developed analytical models for these broadband contributions are first validated with well-defined measurements on several airfoils embedded in an homogeneous flow at low-Mach number. Each instrumented airfoil is placed at the exit of an open jet anechoic wind tunnel with or without a grid generating turbulence upstream of it. Sound is measured in the far field at the same time as the wall-pressure fluctuations statistics close to the airfoil trailing edge and the inlet velocity fluctuation statistics impacting the airfoil leading edge. The models are then compared in some practical cases representative of airframes, wind turbines, and automotive engine cooling modules. The airfoil models of the two mechanisms are then extended to a full rotating machine in open space. The model predictions of both mechanisms are compared with in-flight helicopter measurements and automotive engine cooling modules measurements. In both instances, the turbulence-ingestion noise is found to be a dominant source over most of the frequency range. The self-noise only becomes a significant contributor at high angles of attack close to flow separation.

Nomenclature

B	=	number of blades
b	=	nondimensional parameter in Corcos' model
c	=	airfoil chord length
c_0	=	speed of sound
f	=	frequency
$I = I_1 + I_2$	=	total trailing-edge radiation integral
I_1	=	main trailing-edge scattering radiation integral
I_2	=	leading-edge back-scattering radiation integral
K	=	aerodynamic wave number
$\bar{K}$	=	nondimensional aerodynamic wave number with respect to c
$\hat{K}$	=	nondimensional aerodynamic wave number with respect to k_e
K^*	=	nondimensional aerodynamic wave number with respect to Λ
k	=	acoustic wave number
k_e	=	constant in Von Kármán model
L	=	airfoil span
$\mathcal{L}$	=	generalized airfoil response function
$\mathcal{L}_l$	=	low-frequency asymptote of generalized airfoil response function
$\mathcal{L}_h$	=	high-frequency asymptote of generalized airfoil response function
$l_y(\omega)$	=	spanwise correlation length
$M = U_0/c_0$	=	Mach number based on flow speed
M_t	=	tangential Mach number at radius R_0
M_r	=	relative tangential Mach number
(R, θ)	=	polar coordinates of the observer
R_0	=	fan blade radius
S	=	Sears function
S_{pp}	=	acoustic power spectral density
T_u	=	turbulence intensity
t	=	time
U_c	=	convection speed
U_0	=	flow speed
$\bar{u}^2$	=	streamwise velocity fluctuation
$\boldsymbol{x}$	=	observer position
α_g	=	angle of attack with respect to the mean camber line at the leading edge
$\beta = \sqrt{1 - M^2}$	=	compressibility factor
β_0, β_1	=	constants in exponential correction to Liepmann and Von Kármán models
Γ	=	gamma function
γ^2	=	coherence function
Θ, Ψ	=	observer angular coordinates in the rotor frame
Λ	=	turbulence energy integral scale
ρ_0	=	fluid density
Φ_{pp}	=	wall-pressure power spectral density
Φ_{uu}	=	streamwise velocity power spectral density
Φ_{ww}	=	transverse velocity power spectral density
Ω	=	angular velocity
ω	=	radian frequency
ω_e	=	emission radian frequency

I. Introduction

IN the design process of a new automotive engine cooling fan system, one major quality factor that has to be fulfilled by Valeo is a minimum noise configuration for a given cooling duty point. As Caro and Moreau pointed out [1], the noise radiated by these axial fans is tonal and broadband, both contributions being roughly equal in most configurations. The broadband noise can even be more important in other low-speed axial fans such as the propellers of air conditioning units or the large wind turbines [2]. Several competing mechanisms may contribute to the broadband noise. A first important part is the fan self-noise generated at the blade trailing edges. As quoted by Wright [3], trailing-edge noise always exists and provides

Presented as Paper 3039 at the 10th AIAA/CEAS Aeroacoustics Conference Meeting and Exhibit, Manchester, UK, 10–12 May 2004; received 13 November 2004; revision received 20 February 2006; accepted for publication 11 October 2006.

*Senior Research Engineer and R&D Manager, Engine Cooling Fan Systems Core Competencies Group.

†Professor, Laboratoire de Mécanique des Fluides et Acoustique.

the minimum noise that a spinning fan would produce free of any upstream, downstream, and tip interaction. Another major contribution is the noise due to upstream turbulence impinging on the leading edge, referred to as leading-edge noise here. It comes from the ingestion of large vortical structures such as the ground elongated turbulence ingested by a helicopter tail-rotor, or small scale turbulence shed for instance by the heat exchanger core of a puller automotive engine cooling module. A third mechanism not considered here is the possible vortex shedding due to the trailing-edge bluntness. Finally, the noise radiated by blade-tip vortices and leakage flows can also be important but is ignored in the present study.

The study of leading-edge and trailing-edge noise mechanisms has received much attention mainly in the late seventies and early eighties. Experimentally, it involved measurements of incident velocity fluctuations, wall-pressure fluctuations, and far-field sound on two-dimensional mock-ups of various aerodynamic airfoils in freejet anechoic wind tunnels [4–8]. Theoretical ad hoc models were also developed at the same time [9–16]. More recently, the available experimental data has been used to validate sophisticated numerical prediction methods for trailing-edge aeroacoustics, such as large eddy simulation (LES) [17–19]. Yet, even though these methods are powerful, they do not provide a simple and reliable tool that could be used in an industrial design cycle or could be even applied to a realistic fan configuration. The alternative method presented in the next section is based on analytical techniques [20–22]. Both noise mechanisms and the corresponding formulations are considered in detail. Section III applies the methodology to several airfoils typical of the preceding industrial noise issues. The goal is here twofold: the relative importance of the main acoustic scattering and the secondary back-scattering in each noise mechanism (finite chord effect) is first assessed in various flow conditions and the full simulation is also compared with commonly used asymptotic formulation valid for low- or high-frequencies; the two noise mechanisms are then compared in increasing complex geometries for several subsonic Mach numbers and a broad range of Reynolds numbers. Some focus is given on the controlled diffusion (CD) airfoil designed by Valeo as it provides the test case for the extension of the model to rotating machines as described in section IV. This application also represents the first complete comparison with measurements in a realistic automotive engine cooling module.

II. Noise Mechanisms

Leading-edge noise can be viewed as the scattering of sound of incident turbulence at the geometrical discontinuity of the leading edge. In the same way, trailing-edge noise can be seen as the scattering of turbulent kinetic energy produced in the blade boundary layers into acoustic waves at the geometrical discontinuity of the trailing edge. Strictly speaking, these turbulent fluctuations and the subsequent acoustic pressure fluctuations at an observer location can only be obtained numerically by compressible direct numerical simulations (DNS) or LES that are hardly achievable even on simplified geometries such as two-dimensional airfoils. Moreover, the inherent numerical dissipation of the discretization scheme or the grid skewness often precludes propagating the acoustic waves far from the airfoil. Linearized Euler equations have then been used to propagate the near-field acoustic pressure to the far field while accounting for the external flow. In practical industrial cases, both steps are still computationally too intensive. One has then to resort to a statistical approach, the mean pressure and velocity fields being provided by Reynolds-averaged Navier–Stokes (RANS) simulations. To this end, analytical models have been derived. These models are based on the acoustical analogy and they relate the noise power spectral density (PSD) in the far field at a given observer position and for a given frequency to some statistics in the flow. More precisely, leading-edge interaction noise is deduced from a statistical description of the incident turbulent velocity field [10,11,15] and trailing-edge noise is deduced from a statistical description of the wall-pressure field near the blade trailing edge [12,13]. The models also account for a uniform external flow field at a velocity U_0, contrary to approaches based on Green's functions without external flow [9,14].

A. Trailing-Edge Noise Formulation

First, the trailing-edge noise model relates the PSD of the far-field acoustic pressure to the PSD of the wall-pressure fluctuations close to the trailing edge, a spanwise correlation length, and an acoustical radiation integral. The model is based on the basic scattering of waves by the edge of a half-plane and is applied in an iterative way at both geometrical discontinuities of an airfoil [23]. The main trailing-edge scattering is determined assuming that the airfoil surface extends toward infinity in the upstream direction. Amiet [12] reduced the formulation to this first evaluation and calculated the radiated sound field by integrating the induced surface sources on the actual chord length and the mock-up span, assuming a frozen turbulent field in the boundary layers past the trailing edge. This provides a first evaluation of I, say $I \simeq I_1$. This radiation integral involves both the freestream velocity and the convection speed as parameters. A leading-edge correction fully taking into account the finite chord length (second iteration and correction I_2 to I) has been derived recently [20,22,24]. The predicted sound field, specified to low-Mach number and in the midspan plane, then reads at a given observer location $\boldsymbol{x} = (x_1, x_2, 0) = (R, \theta)$ and for a given radian frequency (or wave number)

$$S_{pp}^{\mathrm{TE}}(\boldsymbol{x}, \omega) = \left(\frac{\sin\theta}{2\pi R}\right)^2 (kc)^2 \frac{L}{2} |I|^2 \Phi_{pp}(\omega) l_y(\omega) \tag{1}$$

In Eq. (1), the origin of coordinates is taken at midspan on the trailing edge. As the observer is in the geometrical far field ($R \gg L, c$), it can be equivalently placed at midchord for a direct comparison with the turbulence-interaction noise model described in the next section. The radiation integral involving both the freestream velocity and the convection speed as parameters, has been derived by Roger and Moreau [20]. Apart from the assumption of a statistically homogeneous pressure field near the trailing edge, the key issue with Eq. (1) is that the angle of attack and the shape of the airfoil cross section only determine the flow features responsible for the sound generation but have no expected effect on the sound radiation. The airfoil is assimilated to a flat plate and the quantity $S_{pp}^{\mathrm{TE}}/(\Phi_{pp} l_y)$ must be nearly invariant. This was verified and the model was validated by a comparison with simultaneous measurements of wall-pressure spectra and far-field noise performed in the Ecole Centrale de Lyon (ECL) anechoic wind tunnels on a thin cambered CD airfoil developed by Valeo [20,21]. The latter mock-up has a chord length of 13.6 cm and a span of 30 cm. The assumption of a homogeneous random pressure field at the trailing edge was also verified over a wide range of geometrical angles of attack and for two different jet widths, which accounted for solidity effects typically found in engine cooling fans [21]. Moreau et al. [25] also emphasized that the actual experimental setup needed be accounted for to reproduce the measured airfoil mean pressure coefficients and therefore to later deduce the boundary layer parameters that will make the wall-pressure spectra nondimensional and useful input data for the statistical model.

B. Turbulence-Interaction Noise Formulation

Equation (1) based on the standard Schwarzschild's solution was first proposed by Amiet to handle the problem of the noise from turbulence impinging on an airfoil [10]. It is equivalent to the application of previously published unsteady aerodynamic theories [26] to acoustic problems. The resulting radiated sound field, specified to low-Mach number and in the midspan plane, then reads at a given observer position $\boldsymbol{x} = (x_1, x_2, 0) = (R, \theta)$ and for a given radian frequency (or wave number)

$$S_{pp}^{\mathrm{TI}}(\boldsymbol{x}, \omega) = \left(\frac{\rho_0 U_0 \sin\theta}{2R}\right)^2 (kc)^2 \frac{L}{2} |\mathcal{L}|^2 \Phi_{ww}(\omega) l_y(\omega) \tag{2}$$

with Φ_{ww} the PSD of the vertical velocity fluctuations, a spanwise

correlation length of the vertical velocity fluctuations impinging the airfoil, and the generalized airfoil response function involving the freestream velocity as a parameter. Again, $\mathcal{L}$ is the sum of a main leading-edge scattering contribution and a trailing-edge back-scattering correction given by Paterson and Amiet's Eqs. (15a) and (15b), respectively [11].

When the radian frequency is small, the response function reduces to the sectional unsteady lift of the airfoil as given by linearized aerodynamics in the limit of small perturbations. Linearized aerodynamics states that the angle of attack and the true airfoil shape only determine the steady lift on an airfoil. On the contrary, the lift fluctuations responsible for the sound radiation are established as if the airfoil was a flat plate with zero angle of attack. The validity of this assumption might be dependent on the Mach number and the Reynolds number. So far, it has been checked in the ECL anechoic wind tunnel for a range of parameters covering low-speed fan noise applications, typically a Mach number around 0.1 and chord-based Reynolds numbers around 2.10^5. All the details on the experimental setup have been recently provided by Moreau et al. [27]. A turbulence-generating grid was placed in the nozzle, ensuring a 5% turbulent intensity impinging on a NACA 0012 airfoil. The geometrical angle of attack of the airfoil was varied from 0 to 20 deg with negligible changes in the far-field sound measured in the airfoil reference frame. The flow was found to remain attached up to the high angle of attack due to both the jet flow deflection and the benefit of the inflow disturbances. The corresponding far-field sound PSD are shown in Fig. 1. Some of the observed remaining differences are attributed to the ignored sound scattering at the nozzle lips [28].

When the PSD of the vertical velocity fluctuations and the spanwise correlation length of the inlet velocity fluctuations are not available, locally homogeneous and isotropic turbulence may be assumed and the expressions for Φ_{ww} and $l_y(\omega)$ are taken from either Von Kármán or Liepmann models as provided in appendix A. It should be emphasized that the transverse PSD is not easily measured. Instead, a single hot wire usually measures the streamwise PSD. The latter can then be fitted with either model for isotropic turbulence and the former is then deduced with the same parameters and used for the leading-edge noise prediction. Figure 2 compares the two PSD for the grid turbulence impinging on the NACA 0012 airfoil. At low-frequencies, the streamwise PSD is about 3 dB higher than the transverse PSD. Φ_{ww} is higher than Φ_{uu} at high-frequencies with the same decay.

Figure 3 compares the streamwise velocity spectra measured at the nozzle exit of the ECL anechoic wind tunnel in the trailing-edge noise experiments [20,21], with the Von Kármán model using the measured low-turbulent intensity of 0.8%. The best fit at low- and medium-frequencies is provided by an integral scale of 0.6 m. So high a value does not correspond to a true grid-turbulence measurement as previously described. It must be thought as a best-fit parameter. In Fig. 3, the sensitivity to the integral scale is also shown. For larger Λ, the threshold frequency at which the velocity spectrum

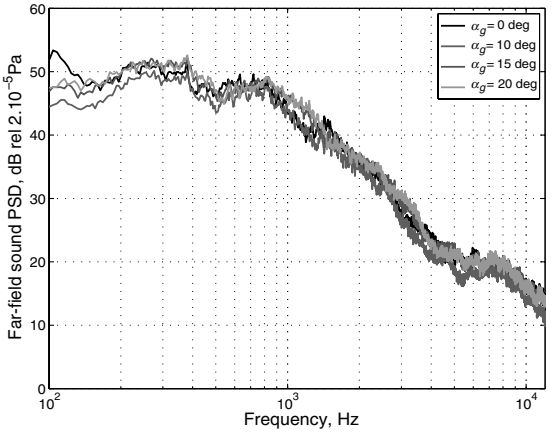

Fig. 1 SPL from NACA 0012 airfoil in 5% turbulent stream at various incidences.

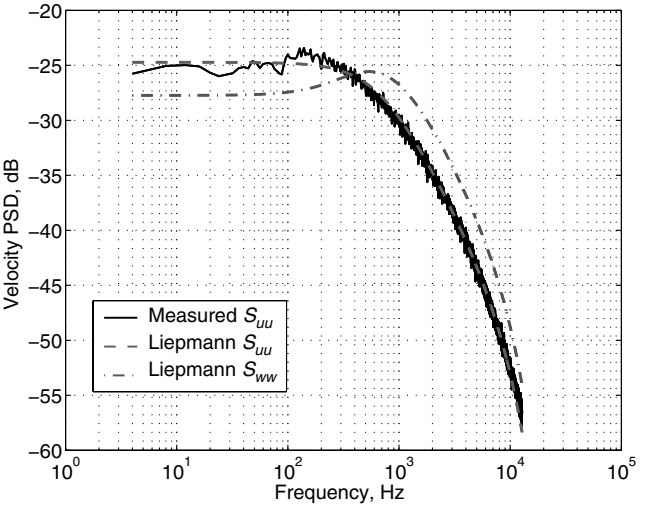

Fig. 2 Comparison of streamwise and transverse velocity PSD (high-frequency correction included).

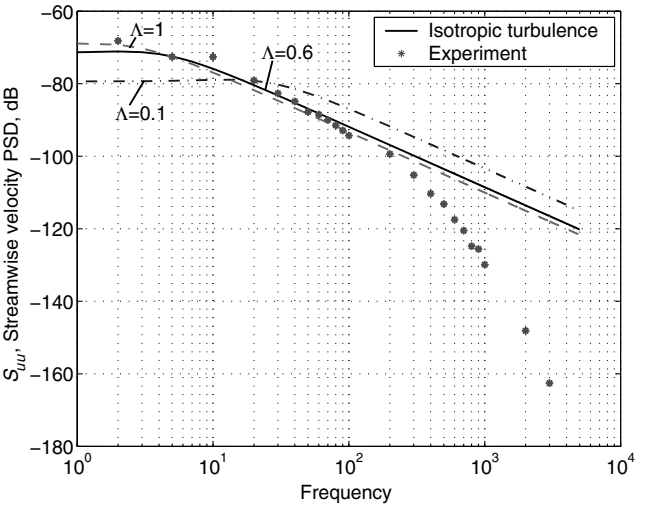

Fig. 3 Comparison of ECL measurements with the original Von Kármán model.

decays moves to frequencies that are too low. For smaller Λ, it shifts to frequencies that are too high. The Liepmann model for both preceding comparisons would predict slightly steeper decays and no significant change in the estimate of the integral scale. The isotropic model overestimates the measurements at higher frequencies. This faster decay at the higher frequencies corresponds to the end of the inertial range and the breakdown due to viscosity, ignored in the aforementioned standard models. In most cases, this part is not radiating efficiently when impinging on an airfoil. However, some simple corrections can be introduced to extend the fitting of model and measurements up to the Kolmogorov scale. If the exponential correction suggested in Appendix A is applied, a very good agreement is obtained with the measured spectrum as shown in Fig. 4. A more physical decay is predicted with the linear argument in the exponential.

In Fig. 5, the Von Kármán model is now compared with the measurements made in the small ECL anechoic wind tunnel behind an automotive engine cooling heat exchanger with a single hot wire at three different speeds [1]. An integral scale of about 1 mm provides the best fit if the measured turbulent intensities are used. The low-frequency levels and the crossings of the spectra for the three speeds (at 1 and 2 kHz) are well reproduced. The slope of the decaying spectra at high-frequencies is again obtained by adding an exponential term with a linear argument. Behind a heat exchanger, the inertial subrange has almost disappeared compared to an isotropic grid turbulence.

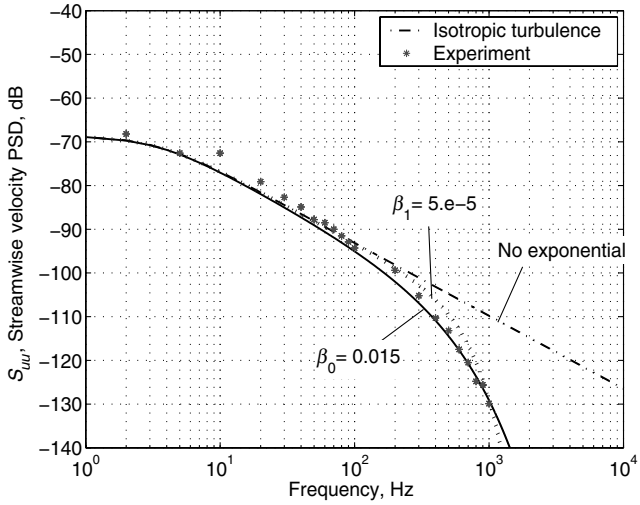

Fig. 4 Comparison of ECL measurements with the corrected Von Kármán model.

To verify the proper implementation of the preceding leading-edge noise model, Fink's experimental data [29] referred by Amiet [10] is considered. In this experiment in the United Aircraft Research Laboratories (UARL) acoustic tunnel, a turbulence-generating grid with known characteristics (a streamwise turbulent intensity between 3.1 and 4.4% and an integral scale of 0.03 m) had been placed upstream of a NACA 0012 airfoil with a chord of 0.457 m and a span of 0.533 mounted between sideplates at zero angle of attack. Third octave sound measurements were made directly above the airfoil. In Fig. 6, these measurements for the five Mach numbers tested by Fink [29] are compared with the results given by Eq. (2) along with the high-frequency approximation given in Appendix B. Similar good agreement as Amiet [10] is found.

To assess the relative importance of the main, leading-edge scattering and the trailing-edge back-scattering, the third octave sound pressure levels (SPL) of each contribution are compared in Fig. 7. The leading-edge contribution dominates in this case and the back-scattering is negligible. The low- and high-frequency approximations of Appendix B are also plotted in Fig. 7. The transition occurs at the anechoic cutoff of the test chamber around 200 Hz and the leading-edge noise is given with a good accuracy by the high-frequency asymptote.

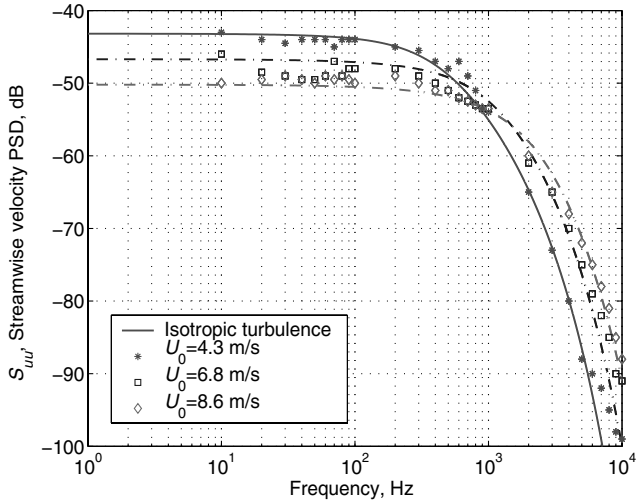

Fig. 5 Comparison of heat exchanger measurements with Von Kármán model for three speeds.

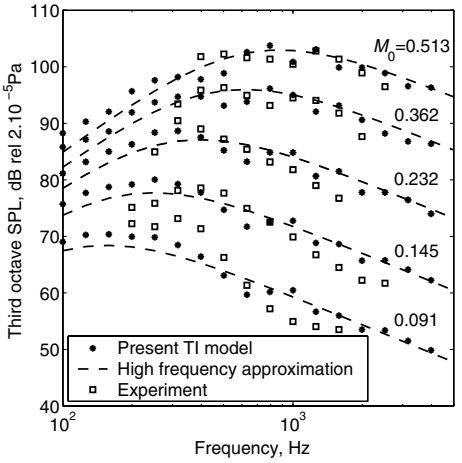

Fig. 6 Comparison of analytical turbulence-interaction (TI) noise models [10] with UARL measurements.

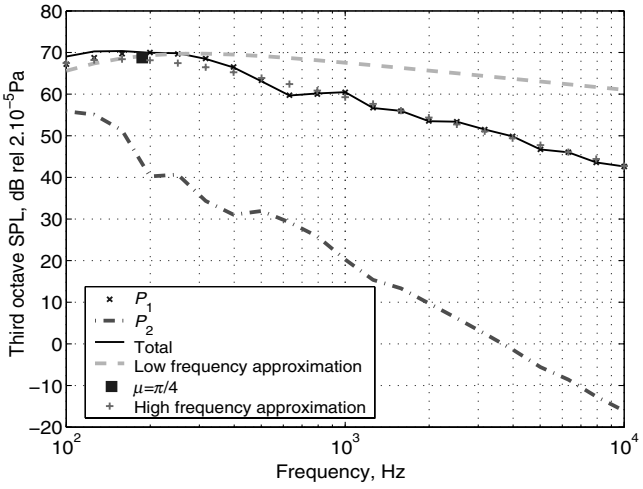

Fig. 7 Contributions to the leading-edge noise prediction at $M_0 = 0.091$ in the UARL experiment.

C. Discrimination Between Trailing-Edge Noise and Turbulence-Interaction Noise

The practical conditions of pure trailing-edge noise are encountered whenever an airfoil is embedded in a quiescent flow, which means a residual inflow turbulence rate below 1%. Wind-tunnel results obtained with a symmetric NACA 0012 airfoil, and mentioned here for the sake of the discussion [30], indicate that as the inflow turbulence rate grows up to 2.5%, the broadband noise turns to be dominated by the impingement of the upstream turbulence, at least in the low- and middle-frequency range. However, trailing-edge noise is still generated by the boundary layer turbulence and presumably by the nearest turbulent eddies in the external flow. As a result, it is in principle impossible to observe pure turbulence-interaction noise. In the analytical models, both mechanisms are considered as perfectly uncorrelated for convenience, which appears questionable at a first glance. In fact, the assumption is compatible with some inspection of the wall-pressure fluctuations measured on an airfoil in a flow with increasing turbulence. Typical results from Arbey [30] are reproduced in Fig. 8. The wall-pressure level is plotted, in arbitrary dB-scale, as a function of the chordwise coordinate and of the turbulence rate, for two frequencies, 100 and 1500 Hz. These values correspond to the limits of the frequency range of the incident velocity fluctuations generated by different grids upstream of the airfoil. For the flow speed 20 m/s considered here, the corresponding values of the parameter $\bar{K} = \omega c/2U_0$ are 1.6 and 23.6, respectively. The rate of turbulence ranges from 2.5 to 12%.

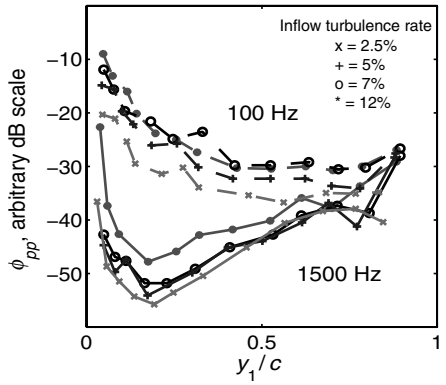

Fig. 8 Chordwise distribution of wall-pressure amplitude (NACA 0012 airfoil, $c = 8$ cm, $U_0 = 20$ m/s).

At low-frequency, wall-pressure fluctuations take their maximum values at the leading edge, then decrease regularly farther downstream, and finally slightly increase again near the trailing edge. Globally, the fluctuation level increases with the turbulence rate over the whole surface except close to the trailing edge. At high-frequency, the maximum wall-pressure is clearly observed at the trailing edge. Furthermore, the chordwise variations appear to be independent of the inflow turbulence rate, as long as the latter remains below 12%, which is quite a high value for most practical applications. Only the area close to the leading-edge is still dominated by the oncoming turbulence.

The aerodynamic wall-pressure is the trace of the vortex dynamics, responsible for the sound generation. These results then show that the distributed sources contributing to trailing-edge noise and turbulence-interaction noise compete differently, depending on frequency and turbulence rate. They also stress that the boundary layer driven wall-pressure fluctuations, and the consequent trailing-edge noise sources, are nearly independent of the turbulence rate in the external flow, especially at high-frequencies. This experimental behavior suggests that the downstream-increasing wall-pressure field in the boundary layer yields the source of pure trailing-edge noise on the one hand, and that the leading-edge concentrated field is associated with the turbulence-interaction noise on the other hand. The two noise mechanisms can then be treated as uncorrelated.

III. Airfoil Results

In this section, the contributions of both mechanisms described in the previous section are combined in several airfoil test cases and compared. The contributions of the leading-edge back-scattering on the trailing-edge noise and the trailing-edge back-scattering on the leading-edge noise are also assessed.

A. Airframe/Wind Turbine Verification Case

The first airfoil case is typical of an airframe or a wind turbine application [12]. It has a chord of 5 m and a span of 40 m. The external flow has a Mach number of 0.3 and the observer is 200 m away above the retarded position of the airfoil. The turbulence impinging on the airfoil is assumed isotropic with a turbulence intensity varying from 1 to 10% and a constant integral scale of 1 m typical of atmospheric conditions. The wall-pressure statistics are taken from the empirical expression given by Amiet [12] from the turbulent wall-pressure spectra over a flat plate of Willmarth and Roos [31]. The spanwise correlation length at the trailing edge is assumed to be given by Corcos' model:

$$l_y(\omega) = \frac{bU_c}{\omega} \tag{3}$$

Finally, the convection speed and correlation length constants in Eq. (3) are given in Table 1. Figure 9 shows the far-field noise levels calculated with the analytical models for the two extreme turbulence intensity cases. Similar numerical results as Amiet [13] are obtained for the low-turbulence case, with a contribution of trailing-edge noise becoming dominant beyond 2000 Hz. For this case, the back-scattering contributions are even more negligible than in the case of Fig. 7 and the transition to the low-frequency approximation for the leading-edge sound is at about 15 Hz. The airfoil is highly noncompact over the whole considered frequency range. For the high-turbulence case, the leading-edge noise becomes the dominant noise source up to 10 kHz.

Table 1 Parameters of airfoil self-noise for different experimental conditions

Airfoil/reference	Constant $1/b$	U_c
Flat plate (Amiet)	0.476	$0.8U_0$
NACA 0012 (Brooks)	0.62	$0.6U_0$
	0.58	$0.6U_0$
Valeo CD (Roger)	0.67	$0.6U_0$

B. NACA 0012 Airfoil Case

The second comparison deals with the experiment of Brooks and Hodgson in the anechoic wind tunnel at NASA Langley Research Center [5]. The airfoil used in this test was a NACA 0012 airfoil with a chord length of 0.6096 m and a span of 0.46 m. The experiment also included several trailing-edge extensions to study the effect of the trailing-edge bluntness. The flow conditions were varied from about 20 to 70 m/s with three different angles of attack, 0, 5, and 10 deg. Surface pressure spectra were measured at the same time as the far-field noise spectra. These measured wall-pressure spectra are used in the present simulation. The corresponding measured convection speed and correlation length constants are again given in Table 1. For the inlet turbulence, turbulence intensities of 0.5 and 1%, more realistic of wind-tunnel conditions, are taken. An arbitrary integral scale of 0.01 m is chosen to stress its potential impact.

Figure 10 compares the two calculated sound contributions with the measured far-field noise at 1.2 m, for the two velocities of 69.5 and 38.6 m/s, and an airfoil with a sharp trailing edge at a 0 deg angle of attack. These conditions have been selected to avoid the noise spectral hump due to vortex shedding. Good agreement is found between the trailing-edge model prediction and the measured sound. Figure 10 also stresses that the leading-edge noise can become dominant very quickly. Even for the low-turbulent intensity 0.5%, the trailing-edge noise only supersedes its leading-edge counterpart above 2–3 KHz at low-speed and above 5 kHz at high-speed. These threshold frequencies are only indicative and will switch to lower frequencies when the exponential dissipation range dominates over the inertial subrange as shown in the next section for the CD airfoil. Nevertheless, such a result emphasizes the importance of measuring

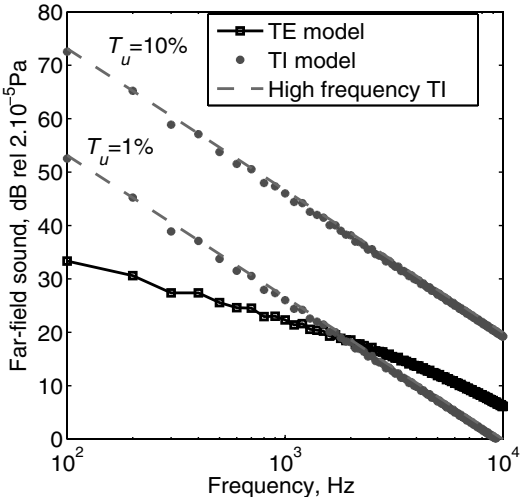

Fig. 9 Trailing-edge noise (TE) compared with TI noise. Simulated airframe/wind turbine case [13].

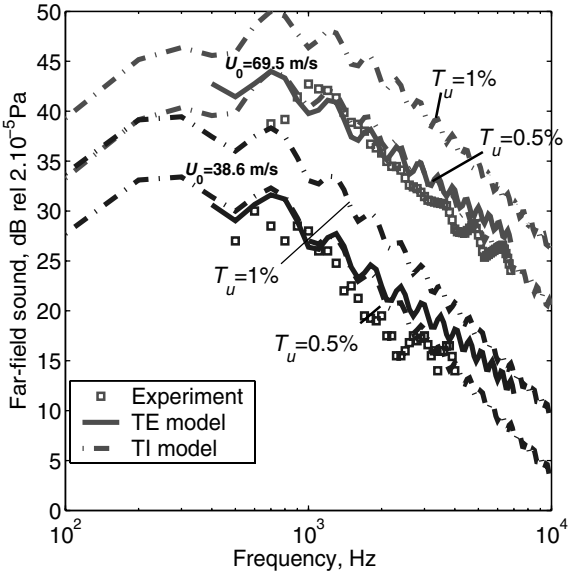

Fig. 10 Trailing-edge noise compared with turbulence-ingestion noise. NACA 0012 test case [5].

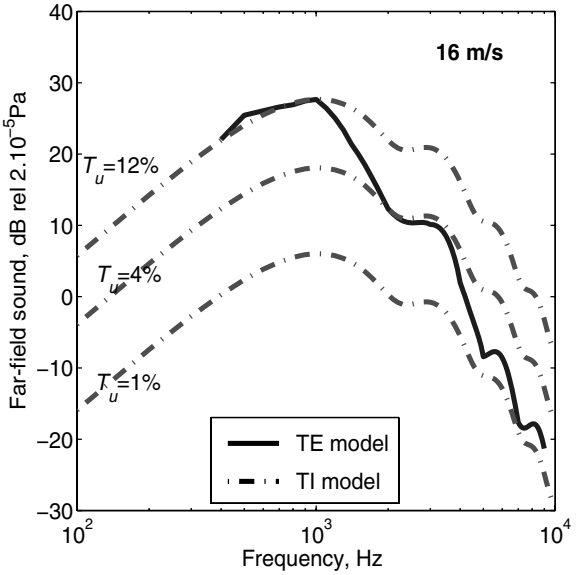

Fig. 12 Comparison of calculated TE and TI noise. Valeo test case in cooling module.

and controlling inlet turbulence for estimating self-noise. For both mechanisms, the main contribution is again the dominant noise source and the back-scattering is negligible. Finally, for these conditions, the transition to the low-frequency approximation for the leading-edge noise is found around 100 Hz.

C. Valeo Controlled Diffusion Airfoil Case

The third comparison deals with the experiment of Roger and Moreau in the ECL anechoic wind tunnels [20,21] performed on the Valeo CD airfoil described in Sec. II.A. The three different flow regimes are considered here [20]: the turbulent boundary layer initiated by a leading-edge separation for a flow velocity 30 m/s, the separated boundary layer with vortex shedding at the trailing edge for a flow velocity 16 m/s, and the laminar boundary layer with Tolmien Schlichting (TS) waves for a flow velocity 10 m/s. The measured wall-pressure spectra are used for the trailing-edge model and the fitted inlet velocity spectrum of Fig. 3 for the leading-edge model.

Figure 11 compares the two calculated sound contributions with the measured far-field noise at 1.3 m above the airfoil, for the aforementioned three velocities of 10, 16, and 30 m/s. In all cases,

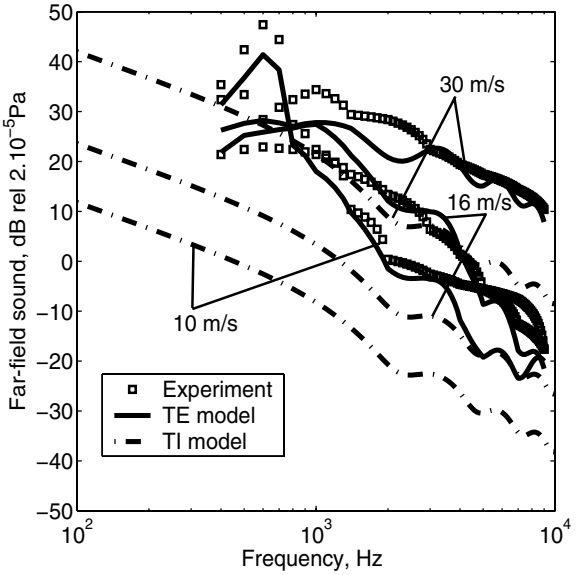

Fig. 11 Trailing-edge noise compared with turbulence-ingestion noise. Valeo test case in ECL experiments.

the leading-edge sound is negligible compared with the trailing-edge noise over the whole frequency range studied in the experiment. This is further emphasized by accounting for the exponential decay at high-frequencies. When such turbulence characteristics are applied to Brooks and Hodgson's experiment [5], the leading-edge sound is also found to be negligible.

We then focus on the sound emitted by the same airfoil in the same flow conditions but behind an engine cooling heat exchanger and the fitted inlet velocity spectra of Fig. 5 are now used. Figure 12 shows both trailing-edge and leading-edge noise predictions for the velocity of 16 m/s with three turbulent intensities encountered in the heat exchanger measurements. Similar plots are obtained for the other two flow conditions. Now the leading-edge noise supersedes the trailing-edge noise at the highest turbulent intensity and beyond 2000 and 10,000 Hz for the other two cases, respectively. Using the proper exponential decay of the velocity spectrum beyond 1 kHz also yields a similar slope in the far-field sound for both mechanisms from 1 to 10 kHz. The highest turbulent intensity case corresponds to a typical distance of 10 mm behind a heat exchanger, which is now frequently accounted in the modern very compact automotive underhood environment. Figure 12 stresses that the turbulence ingestion coming from the heat exchanger may in this case overcome the self-noise generated by the fan itself pulling air through the heat exchanger.

As shown in Fig. 13 for the leading-edge noise and the velocity of 16 m/s, the back-scattering becomes significant below 100 Hz. Beyond this frequency, the main contribution is dominant for both noise mechanisms. Similar results are found for the other flow conditions. Finally, for all conditions, Fig. 13 also shows that the transition to the low-frequency approximation for the leading-edge noise is found around 620 Hz.

IV. Airfoil Directivities

To move from the previous spectra at a single position of the observer above the airfoil to a full-fan prediction, accurate noise directivity must be simulated. This is important to account for the sweep, lean, and twist of a fan blade at a given radial position, which will introduce various orientations of the noise source with respect to the observer.

Directivity has first been validated independently of the flow regimes. To achieve such a goal, the conditions for which the boundary layers are laminar and unstable in the aft part of the airfoil, leading to the onset of TS waves, have been selected. Indeed, due to acoustic back-reaction, self-sustained oscillations occur at discrete frequencies selected by the feedback loop parameters and an isolated tone is associated with wall-pressure fluctuations that are almost

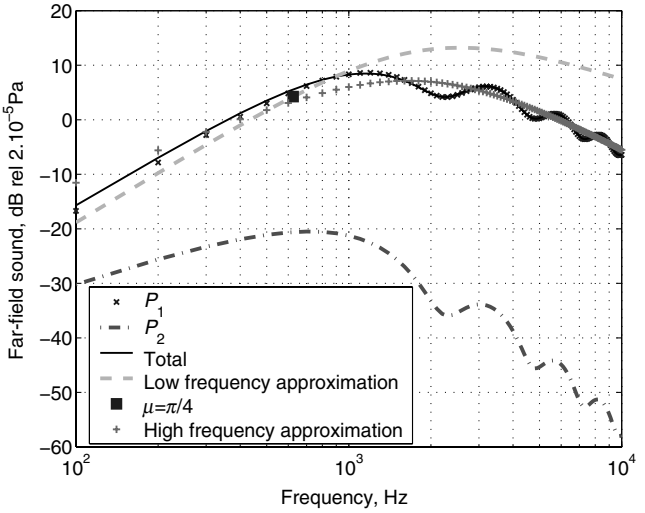

Fig. 13 Contributions to the leading-edge noise prediction at $M_0 = 0.05$ in the ECL experiment.

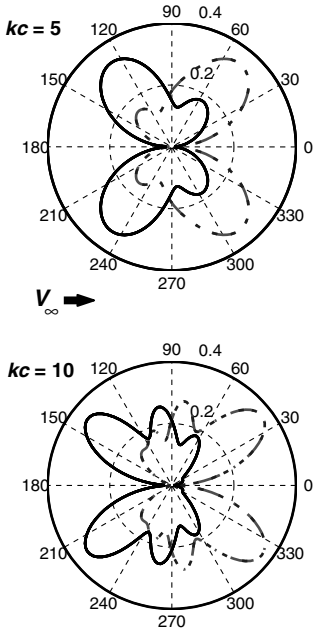

Fig. 14 Computed directivity for both leading-edge (dashed) and trailing-edge noise (solid); dB-scale.

perfectly spanwise-correlated [20]. Therefore, the isolated TS radiation is a nearly two-dimensional process with respect to an observer in the distant midspan plane and, as such, should provide the best comparison between measured and computed directivity patterns. This was done, for instance, with a NACA 0012 airfoil at zero angle of attack in the ECL wind tunnel.

Directivity has then been investigated for the other flow regimes mentioned in Sec. III.C. The Valeo CD airfoil was, for instance, considered in the case of the vortex shedding regime for two flow velocities. Roger and Moreau [20] showed that the experimental directivity integrated over the frequency range 400–10,000 Hz for the 31 m/s velocity compared more favorably with the present finite chord model than with the sine and cardioid results, that can be considered as two opposite asymptotic trends. The aforementioned diffraction at the nozzle lips should account for the remaining discrepancies [28].

Finally, the radiation directivities of both noise mechanisms considered herein are given in Fig. 14 for a Mach number of 0.05. The results are plotted in linear scale, with amplitude adjustment to avoid differences due to the different input data in Eqs. (1) and (2). They are an illustration of the directivity patterns in the midspan plane. Trailing-edge noise sources radiate preferentially upstream and turbulence-interaction noise sources preferentially downstream, as the reduced frequency increases due to noncompactness. The number of lobes is determined primarily by the reduced frequency kc and less importantly by the Mach number.

V. Fan Extension and Results

The airfoil models of Sec. III are extended to a rotating frame by applying them to each blade segment splitting a fan blade. As an isolated airfoil, a rotating blade segment exhibits an attached, a partially, or a fully separated boundary layer at the trailing edge. This boundary layer state can be characterized by well-defined wall-pressure statistics. Similarly, an upstream turbulent flow with well-defined velocity statistics impinges on the rotating blade segment. Therefore, the transfer functions from single-airfoil theories can be applied to predict the noise radiated by a complete fan in the far field, provided that the required information is available at different radii and at the price of a minimum adjustment. The main idea is that the circular motion can be considered locally as tangent to an equivalent translating motion, for which Eqs. (1) and (2) hold. This is only true for sound frequencies much higher than the rotational frequency. Initially developed for high-speed blades of model helicopter rotors in wind-tunnel testing [6,15], the analysis presented here is specified to low-Mach number fans, operating in a medium at rest.

Let (x_1, x_2, x_3) be the instantaneous coordinates of the observer in a reference frame attached to a blade segment at angle Ψ in the rotational plane. At the corresponding instant, the surrounding fluid is moving with respect to the blade with the relative velocity induced by rotation. This velocity is assumed parallel to the chord line according to the weakly loaded airfoil assumption in the linearized theory. Sound propagates toward the observer according to the convected Helmholtz equation expressed in the reference frame (x_1, x_2, x_3). The solution would be exactly given by the single-airfoil formulas providing the convection effects are negligible on the sound propagation. This is particularly the case for the present low-speed fan applications.

Because the blade is moving with respect to the observer, the instantaneous emitted frequency $\omega_e(\Psi)$ at current position $\Psi = \Omega t$ and corresponding to the given frequency received by the observer is determined by the Doppler factor, according to the formula

$$\frac{\omega_e(\Psi)}{\omega} = 1 + M_t \sin\Theta \sin\Psi = 1 - M_r \tag{4}$$

in which $M_t = \Omega R_0/c_0$ is the rotational Mach number. The sound heard at frequency ω is produced by sources on the rotating blade segment having different frequencies depending on their angular position. The resulting spectrum must be calculated by averaging over all possible angular locations of the blade segment and by weighting with the Doppler ratio. This yields the following far-field noise PSD for a fan with B blades

$$S_{pp}(\boldsymbol{x}, \omega) = \frac{B}{2\pi} \int_0^{2\pi} \frac{\omega_e(\Psi)}{\omega} S^{\Psi}_{pp}(\boldsymbol{x}, \omega_e)\, \mathrm{d}\Psi \tag{5}$$

where $S^{\Psi}_{pp}(\boldsymbol{x}, \omega_e)$ denotes the total noise spectrum coming from both mechanisms that would be radiated from the current blade segment at angle Ψ ignoring the Doppler frequency shift. $S^{\Psi}_{pp}(\boldsymbol{x}, \omega_e)$ is precisely what is provided by the single-airfoil formulas. For low-Mach number applications and broadband noise with flat and wide frequency content, the Doppler frequency shift has no significant effect. Yet, it is kept in the calculation for the sake of physical consistency (energy conservation). Equation (5) holds as far as there is no blade-to-blade correlation.

The preceding strip theory given by Eq. (5) has first been validated on the helicopter rotor test case of Schlinker and Amiet [6]. For the self-noise prediction, the values of Φ_{pp}, l_y, and U_c have been taken from [6]. The observer is assumed at 74.5 m on the rotor axis. The results shown in Fig. 15 are similar to those mentioned in [6] even though the more general formulation for a finite aspect ratio airfoil,

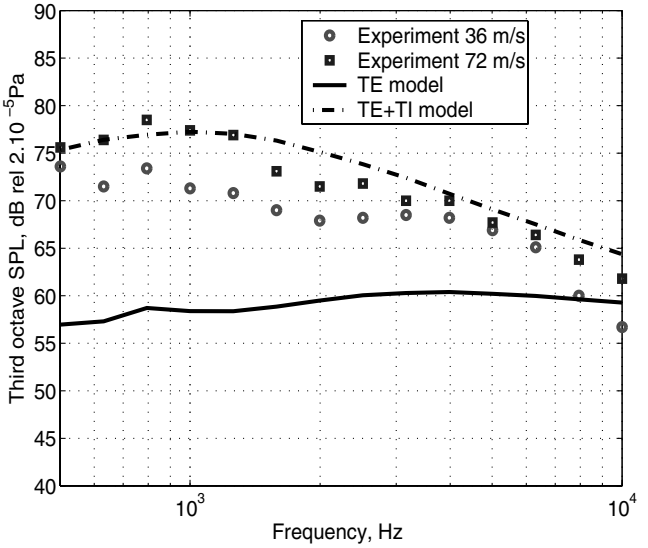

Fig. 15 Comparison of fan broadband model with experiment. NACA 0012 helicopter blade [6] at two different forward flight speeds.

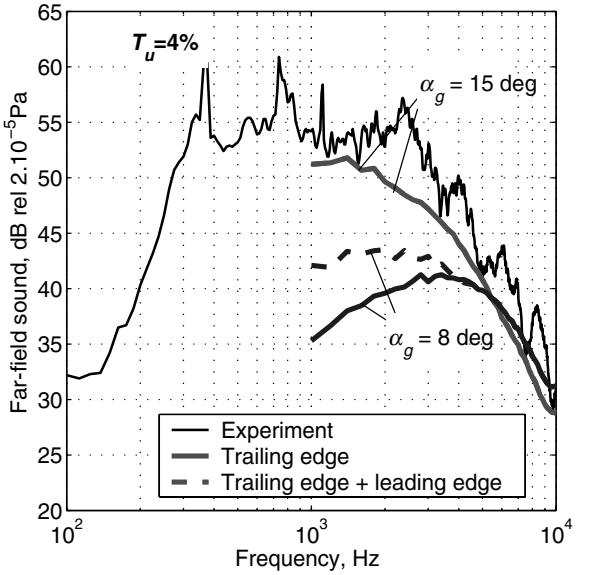

Fig. 16 Comparison of fan broadband model with experiment; effect of Φ_{pp}.

presented in Sec. II.A, has been used here [22] and the forward flight has been neglected. The trailing-edge noise model clearly underestimates the measured noise for both experimental cases. Schlinker and Amiet [6] showed that accounting for the forward flight only induced slightly different predictions, remaining far from the flight data. Setting a low-inflow turbulence modeled by an isotropic turbulence of 1% and an integral scale of 0.04 m provides a much better agreement with the measurements. The overprediction that starts at very high-frequencies comes again from the lack of exponential correction in Liepmann's model used here. This suggests that the turbulence-interaction noise certainly dominates in these helicopter cases.

The model predictions have then been compared with the broadband noise measurements on an automotive engine cooling fan designed by Valeo. The exact fan configuration has been used to yield the proper emission frequencies and the mean inlet flow conditions at each strip have been provided by a three-dimensional RANS simulation. For the self-noise prediction, values of Φ_{pp}, l_y, and U_c must be provided for every segment. This information is hardly available in practice, only for a very limited number of airfoil shapes under specific flow conditions as tested, for example, in Sec. II or computed by more sophisticated methods, such as LES. It has then motivated the search for universal models of the wall-pressure statistics, that relate it to some averaged macroscopic aerodynamic parameters characteristic of the boundary layers developing on the blade. For instance, the wall-pressure PSD at the trailing edge was made nondimensional with respect to the external parameters of the local boundary layer by Moreau and Roger [21]. The displacement thickness value was obtained either from single hot-wire measurements in the near wake or from RANS computations. For l_y, models are still scarce for various flow conditions. The classical Corcos' model as given by Eq. (3) can be referred to in the case of attached turbulent boundary layers and a Gaussian model has been proposed by Roger and Moreau in the case of the nearly separated flow on a loaded airfoil [20].

Figure 16 compares the results using the available experimental Φ_{pp}, l_y, and U_c values at two flow regimes described in Sec. III.C, namely, attached and nearly separated turbulent boundary layers, arbitrarily repeated over the whole span [20,21]. The measured velocity statistics corresponding to a 4% turbulence intensity behind a heat exchanger, as shown in Fig. 5, is also applied over the whole blade span. This corresponds to a heat exchanger in average proximity to the fan system as used in the experiment. Both noise contributions are compared with the far-field PSD measurements with a constant 20 Hz bandwidth of the complete fan system mounted on an engine cooling module in the Valeo semi-anechoic facility. In such an experiment, the microphone was on the fan axis 1 m from the fan system. Both trailing-edge noise calculations collapse nicely at high-frequencies as expected from the wall-pressure spectra and match well with the measured narrow bandwidth spectrum for frequencies beyond 4 kHz. The result for highly loaded blades ($\alpha_g = 15$ deg) also suggests that some of the medium frequency range (between 1 and 4 kHz) could be explained by larger angles of attack on the tip sections than expected from inlet speed triangles due to the tip clearance recirculation flow. For blades closer to design load ($\alpha_g = 8$ deg), the leading-edge noise increases the overall noise levels up to 8000 Hz. On this engine cooling module at design condition, this is most likely the dominant mechanism between 1 and 4 kHz and the trailing-edge noise mechanism will only contribute beyond 4 kHz.

Figure 17 then compares the effect of the turbulence intensity on the noise spectrum for a constant geometrical angle of attack $\alpha_g = 8$ deg. The selected turbulence intensities again correspond to the values of the airfoil case in Fig. 5. They represent a fan system in increasing proximity to the heat exchanger with increasing turbulence intensity. The 12% turbulence intensity case, which

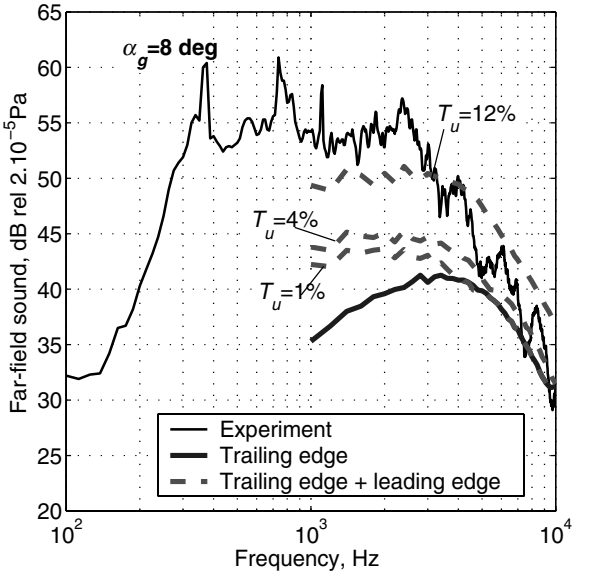

Fig. 17 Comparison of fan broadband model with experiment; effect of incident turbulence intensity.

corresponds to compact engine cooling module trends, suggests that its effect is quite similar to the previous airfoil high angle of attack case. The turbulence-ingestion noise will become dominant over the whole frequency range. For all cases, a significant contribution of the leading-edge noise is again found between 1 and 4 kHz. In both figures, the observed experimental humps not found in the simulations might be due to additional noise mechanisms, presently not accounted for in the model, such as tip flow effects or vortex shedding.

VI. Conclusions

In the present study, two previously developed analytical models for the trailing-edge noise or self-noise, and the leading-edge noise or turbulence-ingestion noise have been formulated, validated, and applied to several industrial configurations, to assess their relative importance.

In the same way as the trailing-edge noise, the leading-edge noise was first validated by comparing the model predictions with well-defined measurements in open jet anechoic wind tunnels. The latter involved several instrumented airfoils placed in a homogeneous flow at low-Mach number with a grid generating turbulence upstream of them. Noise was measured in the far field at the same time as the wall-pressure fluctuations statistics close to the airfoil trailing edge and the inlet velocity fluctuations statistics impinging on the airfoil leading edge. Validation not only involved far-field noise PSD at given spatial locations but also single frequency or frequency-averaged directivities. Three different streamwise fluctuation statistics have then been compared with the analytical Von Kármán or Liepmann models, originally meant for isotropic turbulence, to provide reliable leading-edge noise sources for the present airfoil applications.

The two noise models have then been compared on some practical cases representative of airfoils in anechoic wind tunnels, airframes, wind turbines, and automotive engine cooling modules. For all airfoil applications considered here in the midspan plane, the second order back-scattering of both noise mechanisms has been found to be negligible. The high-frequency approximation of the leading-edge noise has also been found to be adequate for all cases over most of the audible frequency range. Depending on the turbulence intensity and also its spectral content, the leading-edge noise has been found to become dominant, particularly at low- and midfrequencies (below a few kHz).

The airfoil broadband noise model has then been extended to a full rotating machine in open space for both noise mechanisms, assuming a strip theory along the blade and a locally rectilinear fluid motion. In typical helicopter applications, the turbulence-ingestion noise quickly dominates the blade self-noise, except at very high-frequency beyond 10 kHz. Similarly, in engine cooling applications, when the fan system gets too close to the heat exchanger, the turbulence intensity impacting the fan blades gets high and the turbulence-ingestion noise becomes larger than the fan self-noise over most of the frequency range. Local high angles of attack on the fan blade will generate trailing-edge noise that could also be significant.

Appendix A: Isotropic Turbulence Models

The two most widely used models of isotropic turbulence are the Liepmann and Von Kármán models. Details of the derivation of the corresponding energy spectrum can be found in any reference turbulence textbook. Amiet [10] provides the relationship between the energy spectrum and the PSD of the vertical velocity fluctuations and consequently the correlation length [Amiet's Eq. (19) [10]].

On the one hand, the PSD and the cross-correlation length read for the Liepmann model

$$\Phi^L_{ww}(\omega) = \sqrt{\frac{\overline{u^2}}{U_0^2}}\frac{\Lambda}{2\pi}\frac{1+3K^2\Lambda^2}{(1+K^2\Lambda^2)^2}$$

$$l^L_y(\omega) = \frac{3\pi\Lambda}{2\sqrt{1+K^2\Lambda^2}}\frac{K^2\Lambda^2}{1+3K^2\Lambda^2}$$

with $\sqrt{\overline{u^2}/U_0^2}$ as the streamwise turbulent intensity. To fit the hot-wire measurements, the PSD of the horizontal streamwise velocity fluctuations is also needed. It reads

$$\Phi^L_{uu}(\omega) = \sqrt{\frac{\overline{u^2}}{U_0^2}}\frac{\Lambda}{\pi}\frac{1}{(1+K^2\Lambda^2)}$$

On the other hand, the PSD and the cross-correlation length read for the Von Kármán model

$$\Phi^K_{uu}(\omega) = \sqrt{\frac{\overline{u^2}}{U_0^2}}\frac{\Lambda}{\pi}\frac{1}{(1+\hat{K}^2)^{5/6}}$$

$$\Phi^K_{ww}(\omega) = \sqrt{\frac{\overline{u^2}}{U_0^2}}\frac{\Lambda}{6\pi}\frac{3+8\hat{K}^2}{(1+\hat{K}^2)^{11/6}}$$

$$l^K_y(\omega) = \frac{8\Lambda}{3}\left(\frac{\Gamma(1/3)}{\Gamma(5/6)}\right)^2\frac{\hat{K}^2}{(3+8\hat{K}^2)\sqrt{1+\hat{K}^2}}$$

$$\text{with } k_e = \frac{\sqrt{\pi}}{\Lambda}\frac{\Gamma(5/6)}{\Gamma(1/3)}$$

$$\hat{K} = \frac{K}{k_e}$$

To improve the fit with hot-wire measurements, the preceding energy spectra can be corrected to account for the faster decay at high-frequencies. Two physical exponential dependences have been adopted here from the known energy spectrum for isotropic turbulence:

$$\bar{\Phi}^i_{ww}(\omega) = \Phi^i_{ww}(\omega)e^{-\beta_0 K^*} \quad \text{or} \quad \bar{\Phi}^i_{ww}(\omega) = \Phi^i_{ww}(\omega)e^{-\beta_1 (K^*)^2}$$

$$\forall\ i = L, K$$

with $K^* = K\Lambda$ for the Liepmann model and $K^* = \hat{K}$ for the Von Kármán model.

Appendix B: Asymptotic Response Functions

As quoted by Amiet [10], the parameter MK/β^2 which accounts for the combined effect of Mach number and reduced frequency, delimits several ranges for which approximations to the preceding formula for the generalized airfoil loading can be derived.

For $MK/\beta^2 < \pi/4$, a low-frequency asymptote can be derived [Paterson and Amiet's Eq. (11) [11]]:

$$\mathcal{L}_l = S\left(\frac{K}{\beta^2}\right)\frac{e^{-iK}}{\beta}$$

For $MK/\beta^2 \gg 1$, a high-frequency asymptote can be derived [Amiet's Eq. (44) [10]]:

$$\mathcal{L}_h = \frac{-i}{\pi K\sqrt{M}}$$

References

[1] Caro, S., and Moreau, S., "Aeroacoustic Modeling of Low Pressure Axial Flow Fans," AIAA Paper 2000-2094, July 2000.
[2] Hubbard, H. H., and Shepherd, K. P., "Aeroacoustics of Large Wind Turbines," *Journal of the Acoustical Society of America*, Vol. 89, No. 6, 1991, pp. 2495–2507.
[3] Wright, S. E., "Acoustic Spectrum of Axial Flow Machines," *Journal of Sound and Vibration*, Vol. 45, No. 2, 1976, pp. 165–223.
[4] Blake, W. K., "Statistical Description of Pressure and Velocity Fields at the Trailing Edge of a Flat Strut," David Taylor Naval Ship Research and Development Center Rept. 4241, Bethesda, Maryland, Dec. 1975.
[5] Brooks, T. F., and Hodgson, T. H., "Trailing Edge Noise Prediction from Measured Surface Pressures," *Journal of Sound and Vibration*, Vol. 78, No. 1, 1981, pp. 69–117.
[6] Schlinker, R. H., and Amiet, R. K., "Helicopter Trailing Edge Noise,"

NASA CR-3470, 1981.
[7] Arbey, H., and Bataille, J., "Noise Generated by Airfoil Profiles Placed in a Uniform Laminar Flow," *Journal of Fluid Mechanics*, Vol. 134, 1983, pp. 33–47.
[8] Garcia, P., and Gérard, P., "Bruit d'un Profil Dans un Écoulement," ONERA TP 1984-155, Nov. 1984; also *La Recherche Aérospatiale* (English version), Vol. 3, 1989, pp. 1–7.
[9] Ffowcs Williams, J. E., and Hall, L. H., "Aerodynamic Sound Generation by Turbulent Flow in the Vicinity of a Scattering Half-Plane," *Journal of Fluid Mechanics*, Vol. 40, No. 4, 1970, pp. 657–670.
[10] Amiet, R. K., "Acoustic Radiation from an Airfoil in a Turbulent Stream," *Journal of Sound and Vibration*, Vol. 41, No. 4, 1975, pp. 407–420.
[11] Paterson, R. W., and Amiet, R. K., "Acoustic Radiation and Surface Pressure Characteristics of an Airfoil due to Incident Turbulence," NASA CR 2733, 1976.
[12] Amiet, R. K., "Noise Due to Turbulent Flow Past a Trailing Edge," *Journal of Sound and Vibration*, Vol. 47, No. 3, 1976, pp. 387–393.
[13] Amiet, R. K., "Effect of the Incident Surface Pressure Field on Noise Due to Turbulent Flow Past a Trailing Edge," *Journal of Sound and Vibration*, Vol. 57, No. 2, 1978, pp. 305–306.
[14] Howe, M. S., "Review of the Theory of Trailing-Edge Noise," *Journal of Sound and Vibration*, Vol. 61, No. 3, 1978, pp. 437–465.
[15] Paterson, R. W., and Amiet, R. K., "Noise of a Model Helicopter Rotor Due to Ingestion of Turbulence," NASA CR 3213, 1979.
[16] Brooks, T. F., Marcolini, M. A., and Pope, D. S., "Airfoil Self-Noise and Prediction," NASA RP-1218, 1989.
[17] Wang, M., and Moin, P., "Computation of Trailing-Edge Flow and Noise Using Large-Eddy Simulation," *AIAA Journal*, Vol. 38, No. 12, 2000, pp. 2201–2209.
[18] Manoha, E., Delahay, C., Sagaut, P., Mary, I., Ben Khelil, S., and Guillen, P., "Numerical Prediction of the Unsteady Flow and Radiated Noise from a 3D Lifting Airfoil," AIAA Paper 2001-2133, 2001.
[19] Oberai, A., Roknaldin, F., and Hughes, T. J. R., "Computation of Trailing Edge Noise Due to Turbulent Flow over an Airfoil," *AIAA Journal*, Vol. 40, No. 11, 2002, pp. 2206–2216.
[20] Roger, M., and Moreau, S., "Trailing Edge Noise Measurements and Prediction for Subsonic Loaded Fan Blades," *AIAA Journal*, Vol. 42, No. 3, 2004, pp. 536–544.
[21] Moreau, S., and Roger, M., "Effect of Airfoil Aerodynamic Loading on Trailing Edge Noise Sources," *AIAA Journal*, Vol. 43, No. 1, 2005, pp. 41–52.
[22] Roger, M., Moreau, S., and Guedel, A., "Broadband Fan Noise Prediction Using Single Airfoil Theory," *Noise Control Engineering Journal*, Vol. 54, No. 1, 2006.
[23] Landahl, M., *Unsteady Transonic Flow*, Pergamon, NY, 1961.
[24] Roger, M., and Moreau, S., "Back-Scattering Correction and Further Extensions of Amiet's Trailing Edge Noise Model, Part 1: Theory," *Journal of Sound and Vibration*, Vol. 286, No. 3, 2005, pp. 477–506.
[25] Moreau, S., Henner, M., Iaccarino, G., Wang, M., and Roger, R., "Analysis of Flow Conditions in Free-Jet Experiments for Studying Airfoil Self-Noise," *AIAA Journal*, Vol. 41, No. 10, 2003, pp. 1895–1905.
[26] Adamczyk, J. J., "Passage of an Infinite Swept Airfoil Through an Oblique Gust," NASA CR 2395, 1974.
[27] Moreau, S., Roger, M., and Jurdic, V., "Effect of Angle of Attack and Airfoil Shape on Turbulence-Interaction Noise," AIAA Paper 2005-2973, May 2005.
[28] Roger, M., and Moreau, S., "Diffraction and Refraction Effects in Trailing-Edge Noise Free-Jet Experiments," *CFA/DAGA 2004 Congress*, pp. 821–822.
[29] Fink, M. R., "Experimental Evaluation of Theories for Trailing Edge and Incidence Fluctuation Noise," *AIAA Journal*, Vol. 13, No. 11, 1975, pp. 1472–1477.
[30] Arbey, H., "Contribution à l'Étude des Mécanismes de l'Émission Sonore de Profils Aérodynamiques Placés Dans des Écoulements Sains ou Perturbés," Ph.D. Dissertation in Acoustics, No. 81-47, Univ. Claude Bernard, Lyon, France, Sept. 1981.
[31] Willmarth, W. W., and Roos, F. W., "Resolution and Structure of the Wall Pressure Field Beneath a Turbulent Boundary Layer," *Journal of Fluid Mechanics*, Vol. 22, No. 1, 1965, pp. 81–94.

K. Ghia
Associate Editor